Computers and Electrical Engineering 104 (2022) 108405

Contents lists available at ScienceDirect

Computers and Electrical Engineering

journal homepage: www.elsevier.com/locate/compeleceng

COVID-19 identification in chest X-ray images using intelligent multi-level classification scenario

R.G. Babukarthik [a], Dhasarathan Chandramohan [b,*], Diwakar Tripathi [b], Manish Kumar [b], G. Sambasivam [c]

[a] Department of Computer Science and Engineering, Dayananda Sagar University, Bangalore 560078, India
[b] Department of Computer Science & Engineering, Thapar Institute of Engineering & Technology, Patiala, Punjab, India
[c] School of Computing Science and Engineering, VIT Bhopal University, Madhya Pradesh, India

ARTICLE INFO

Keywords:
Genetic deep learning convolutional neural network
Huddle particle swarm
Optimization
COVID-19
Pneumonia
Genetic algorithm

ABSTRACT

COVID-19 is an evolving respiratory transmittable disease, and it holds all daily activity worldwide as a global pandemic. It appeared in the city of Wuhan (China) in November 2019 and slowly started spreading to the rest of the world. The number of cases keeps increasing drastically, leading to a shortage of medical resources and testing kids worldwide. As the physicians facing this problem, several scientists and specialists in Artificial Intelligent (AI) are rendering their support to healthcare professionals in the early detection of COVID-19 using chest X-ray image samples to determine the level of severity at a low cost. This paper proposed Genetic Deep Learning Convolutional Neural Network (GDCNN) architecture that includes Huddle Particle Swarm Optimization as an alternative to Gradient descent. Huddle PSO performs better when clubbed with GDCNN architecture. Based on publicly available datasets, trained chest X-ray images are used to predict and identify various pneumonia diseases. The proposed model performed better with an accuracy of 97.23%, a sensitivity of 98.62%, specificity of 97.0%, and precision of 93.0%. The proposed model act as a tool for earlier detection of COVID-19. In the future, we plan to apply the proposed model for the larger dataset and to predict various lung diseases.

1. Introduction

The new coronavirus started spreading in Wuhan from China and has drastically stretched worldwide since January 2020. The outbreak has created the World Health Organization (WHO) to announce a "Public Health Emergency of International Concern" on the last of January 2020. In February 2020, WHO named the novel coronavirus (COVID-19). Till the 1st of August 2020, 18902735 cases have been affected and confirmed death around 709511 around 216 countries. The recovered are 12547767 cases, thus in the USA, the total cases involved are 5095524, Brazil 2, 967,064, India 2,088,611, Russia 877,135, South Africa 545,476, Mexico 469, 407 and in Peru it is 463,875 has been reported as of now. A significant effect is needed to identify the disease at the initial stage. Some precautionary steps must be followed to prevent others from getting an infection, as no vaccine is available. The spread of disease is controlled by quarantining the affected patients, and ventilators are provided in severe cases. The pandemic situation causes all health

* Corresponding author.
E-mail addresses: r.g.babukarthik@gmail.com (R.G. Babukarthik), pdchandramohan@gmail.com (D. Chandramohan), diwakarnitgoa@gmail.com (D. Tripathi), mk9309@gmail.com (M. Kumar), gsambu@gmail.com (G. Sambasivam).

https://doi.org/10.1016/j.compeleceng.2022.108405
Received 30 January 2022; Received in revised form 17 September 2022; Accepted 22 September 2022
Available online 26 September 2022

organizations at considerable risk as only limited bed facilities are available. Furthermore, the Intensive Care Units are also facilitated with minimal ventilators. Thus from a clinical aspect, COVID-19 diseases cause severe pneumonia in the health care system, like SARS-CoV. Some of the symptoms due to pneumonia are dry cough, fever, difficulty breathing, and exhaustion. Severe cases also lead to renal failure; in the worst case, it leads to death. Recently, several patients have been affected by COVID-19 as they are asymptomatic. That is, COVID-19 infects most people without any indications of symptoms. These, in turn, lead to the drastic spread of the disease to other people, Goundar S. et al. [1] Data analysis and classification to predict the student's performance in the undergraduate computing branch and suggest an approach for reducing student dropouts. In Italy, it is observed that Vo Euganeo, which is 50km west of Venice, has been completely shut down. Furthermore, it is being discovered that among several inhabitants who have been given pharyngeal swabs, about 50-75% are positive without any symptoms [2]. The solution available to identify the COVID-19 infected person has collected the swab and needs to analyze biological material via polymerase chain reaction [3]. A swab is tested for a patient who shows symptoms. Thus, asymptomatic symptoms are difficult to identify [4].

Early diagnosis of COVID-19 is confirmed with the help of polymerase and chain reaction. Pneumonia in the infected patients is identified using Computed Tomography (CT) and chest X-ray images. Moreover, the pattern is abstemiously characteristic is recognized by the human eye [5].

COVID-19 transmission rate depends on reliably detecting affected patients with fewer false negatives. In other words, if the false positives are more infrequent, it prevents the patient from exposing them to quarantine and unnecessarily reduces the burden on the health care system. There is no need to tell the patient to quarantine. Proper infection control and earlier disease detection empower the essential supportive care needed by COVID-19 patients. Para-clinical and clinical features of COVID-19 details are discussed by Chinese researchers at the end of January 2020. It states that the infected patient's chest CT images have a bilateral association [6]. Bilateral sub-segmental and multiple lobular areas alliance the significant findings in CT images of those admitted to the Intensive Care Unit (ICU). In the later stage chest, CT images revealed ground-glass opacity with determined amalgamation.

X-ray and CT images of the chest indicate signs of various pneumonia. Meanwhile, the World Health Organization (WHO) provided several supplementary diagnosing protocols for COVID-19. Test diagnosis is performed using Real-Time reverse Polymerase Chain Reaction (RRT-PCR) [7,8]. The biological samples, such as blood or sputum, are collected from the affected patients, and results are available within a couple of hours or a day [9,10]. The easiest way of diagnosing COVID-19 is using radiological imaging [11,12]. An in-depth study of the various state-of-the-art models designed for identifying COVID-19 is ready. The Genetic Deep Learning Convolutional Neural Networks model, GDCNN, is proposed based on that. The tool helps to detect automatically detect COVID-19, and it is beneficial to radiologists in exact prediction, thereby reducing the delay in the rapid spread of novel coronavirus.

The proposed GCDNN model takes chest X-ray images as an input, and the proposed model is trained on 5000 chest X-ray image samples collected worldwide. The dataset chosen is publicly available and is open-source. The accuracy of the prediction is compared with other existing models. The contribution of the paper is précised as follows:

- Developing a Genetic Deep Learning Convolutional Neural Network model for exact prediction of patients having COVID-19 and other pneumonia within a short time is helpful in early diagnosis.
- Empirical analysis of the proposed GDCNN model is performed to classify the various pneumonia diseases.
- The proposed model's performance is tested for its effectiveness and evaluated by comparing it with other existing models.

The remaining paper is organized as follows. Section 2 states the related work on developing models for earlier detection of COVID-19. Section 3 presents the detailed design of the proposed GDCNN architecture and usage of Huddle Particle Swarm Optimization (PSO) as an alternative to Gradient descent. Section 4 details the dataset used experimental setup and the performance discussion of the proposed model. Section 5 describes the conclusion and future research.

2. Related works

Chest X-ray images are quick interpretations in the diagnosis of COVID-19. Several scientists used deep learning models to detect COVID-19 using x-ray images. Wang et al. [13] proposed COVID-Net, a deep convolutional neural network design for diagnosing patients with COVID-19 using chest x-ray images. The dataset includes image classes like COVID-19 infection, pneumonia bacterial, pneumonia viral, and standard or healthy person (non-COVID19 condition). The proposed model achieved an accuracy of 83.5% for 4-classes, with an overall accuracy of 92.4%. Hemdan et al. [14] suggested the COVIDX-Net model for detecting COVID-19 using chest X-ray images. The proposed model consisting of seven deep learning architectures such as VGG19, MobileNetV2, DenseNet201, Xception, ResNetV2, InceptionV3 and InceptionResNetV2. The proposed model is validated for a dataset set of 50, comprising 25 COVID-19 and normal (non-COVID-19 infection). Furthermore, the analysis shows that DenseNet and VGG19 had performed similarly to F1scores of 0.91 for COVID-19 and 0.89 for normal. InceptionV3 model with the poor performance of F1 scores with 0.00 for COVID-19 and 0.67 for normal. Kumar et al. [15] introduced a system for detecting COVID-19 using a deep convolutional network with X-ray images. The dataset is obtained from an open repository such as Kaggle, GitHub, and Open-I repository, with and prediction accuracy of 95%.

Chen et al. [16] introduced the UNet++ model in deep learning to detect COVID-19 and obtained an overall accuracy of 98.85% using the dataset of size 51 COVID-19-affected patients. The dataset is collected from Renmin Hospital belongs to Wuhan University. The major drawback of the proposed techniques is that only COVID-19 patients are taken. That is, healthy patients are not considered. Furthermore, the details of network predictions are not explained. Net deep learning-based model for the prediction of COVID-19 achieved an accuracy of 92%. The detection process is performed by introducing a deep learning model for the detection of

COVID-19, and the method is similar to Chin et al. without considering healthy patients. An accuracy of 73.1% is achieved, and the dataset is taken from two different institutions. Moreover, the dataset consists of 99 x-ray samples, with 44 cases reporting COVID-19 disease and 55 patients with another kind of pneumonia. Xu et al. [17] stated an approach for detecting COVID-19 using a deep learning model and obtained an accuracy of 86.7%. The dataset consists of 618 chest X-ray images. A three-dimensional deep learning convolutional neural network technique is followed to design the model's prediction. The first network is ResNet23, and the second and third networks are the first network's variants and have various convolutional layers. Zhang et al. [18] proposed a DenseNet network model to predict COVID-19 RNA sequences. Beck et al. [19] used a deep learning model for proteins which enhances for creation of new vaccines. Hemdan et al. [20] introduced COVIDX-Net for detecting the variant by using chest X-ray images. An accuracy of 90% shows the illustration of modern thinking by testing a dataset consisting of 50 samples, of which 25 are COVID-19-affected patients, and the remaining 25 are healthy patients.

Butt et al. [21] proposed two models for classifying COVID-19 images and achieved an accuracy of 86%. The first network model is designed on ResNet23, and the second model is based on the variation of the first one by adding a location attention mechanism with the whole connection layer. The dataset consists of 1710 chest CT image samples, of which 357 are COVID-19, 963 are not related to infection, and 390 Influenza-A-Viral pneumonia. Babukarthik et al. [22] proposed a Genetic Deep Learning Convolutional Neural Network for earlier detection of COVID-19 and obtained an accuracy of 98.84% with multilevel classification. The major problem with this technique is that training a model is time-consuming, and the number of iterations is more for fitness evaluation. Rostami et al. [23] used blood test samples to predict the COVID-19 diagnosis as a human-computer interaction by adapting an Artificial Intelligence-based technique. Decision forest and tree methods consideration for feature selection. The author used radiotherapy for periodic monitoring by Clough et al. [24] to detect the lung status of COVID-19. CBCT image therapy is tested in all circumstances to identify the visible part of the patient lungs early. SMILES dataset is used for decoding and individual encoding molecule. The significant outcome of the proposed techniques is an anti-viral medication that is 2019-nCoV 3C proteinase used for treating HIV/AIDS. From the study, it is clear that a novel approach is required for the earlier prediction of COVID-19. Based on state-of-the-art, a new architectural model is needed to be designed for various classifications of pneumonia diseases. Alternative to gradient descent novel algorithm is vital for optimum search. Tripathi et al. [25] discussed analyzing different ensemble learning techniques for comprehensive classification and ensemble approaches with combinations tested under comparative benchmarks.

3. Preliminary

3.1. Alternative to gradient descent

One of the fascinating ideas in machine learning is gradient descent which minimizes the cost function provided. Furthermore, this algorithm continuously takes phases of the highest descending slope, in the theoretical aspect reaching a minimum after some consecutive steps. Cauchy was discovered in 1847, and after a few years, it is expanded by Haskell Curry in 1944 to solve non-linear optimization problems. Gradient descent has been used in various fields, such as linear regression and deep neural networks. Repurposing gradient descent in the form of backpropagation has made a significant breakthrough in machine learning, yet optimization of neural networks is leftover as an unsolved problem. So many of them on the internet are eager to announce that 'gradient descent sucks,' but still, gradient descent has a few issues some of them are.

- Often the optimizers get held up with the local minima. The above problem is overcome by using momentum. Thereby it processes the optimizers above large hills. The error space is further reduced by batch normalization or stochastic gradient descent. However, local minima remain the primary reason for several branching problems in the case of neural networks.
- The optimizer attracted the local minima. Even though it takes several measures to overcome the problems, it takes more time. Significant factor involvement leads to a slow convergence rate in gradient descent, even in the case of larger datasets.
- During the initialization process, gradient descent is much more sensitive. Thereby, the two local minima are tested instead of the first to validate the optimal performance of all functions. Initial achievement is verified with the optimizer with the appropriate initialization process and takes place randomly.
- It is clear that learning rates indicate how risky and confident the optimizer is; setting a high learning rate may cause to manage global minima, while assessing low learning leads to runtime to the setback. Several learning rates are developed to solve the above issues, but choosing them is very difficult.
- Gradient descent problems face some set back like exploding or vanishing gradient problems, although it exhibits an inability to handle non-differentiable functions.

An in-depth study of gradient descent has proposed various solutions, like variations in gradient descent and other solutions based on network architecture. As gradient descent is the most widely used doesn't mean it is the best solution. Some of the further gradient descent, like Adagrad or Adam and batch normalization, perform better. The primary reason is to focus on specific interesting optimization methods that fit well and to increase the performance of the deep neural network, which can work well in all scenarios.

Huddle PSO is an attractive idea with tremendous advantages, as it is less subtle to initialization than other techniques. Furthermore, communication among the particles to search for solutions is more efficient in the case of large and sparse areas.

Some may think more population-based techniques are computationally expensive than gradient descent optimizers. Still, it is not so, as the Huddle PSO algorithm is non-rigid and open. The research gap is mainly due to the advantage of the evolution algorithm, such as it is easy to control the number of the particles, corresponding to the speed they move. Finally, the volume of information is

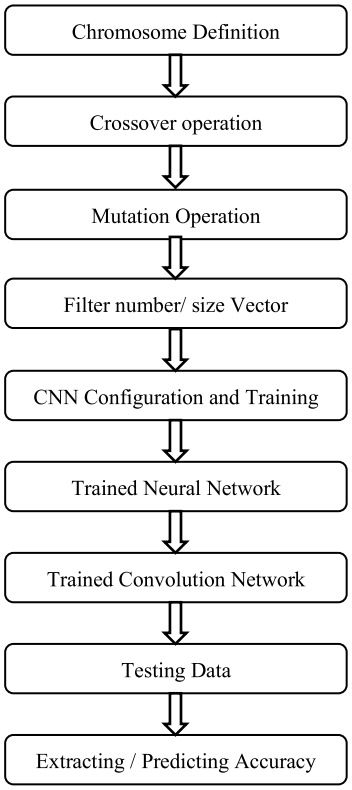

Fig. 1.1. Prediction Workflow.

shared globally, in the same aspect as tuning the learning rates in the deep neural network.

4. Proposed work

To identify the abnormality in users' activity and early prediction of COVID-19 among medicated users. A novel approach of Genetic Deep Convolutional Neural Network (GDCNN) architecture is proposed as a hybrid GDCNN and Huddle PSO. Multi-level classification is performed based on edema, fibrosis, effusion, COVID-19, emphysema, pneumonia, and routine. The hybrid model with Huddle Particle Swarm Optimization algorithm (Huddle PSO) as an alternative to gradient descent.

Prediction workflow of infection and control measures need to be initiated as the outcome of the cycle illustrated in Fig. 1.1.

4.1. Formalization

Dataset consisting of training sample $D = \{X, T\}$ of size N_{size}, chest X-ray image samples $X = \{x_1, x_2, x_3, x_4, \ldots x_{N_{size}}\}$, and truth tables $T = \{t_1, t_2, t_3, t_4, \ldots t_{N_{size}}\}$. Classification of various pneumonia cases $t_1 = \{0, 1, 2 \ldots 14\}$ and the classifier is stated by parameterized by weight w. Y Denotes the output which depends on T that is function***to get the final predicted values. Training is an iterative process for finding a set of weight parameters g: $Y \rightarrow T$. Thus minimizing the average loss function on the training dataset.

$$Loss(w, X) = \frac{1}{N_{size}} (f^w(x_i).(t_i) \tag{1}$$

Where class $y_i = f^w(x_i)$ the output of the decision and the predicted loss function of label and table is represented by

$$loss(y_i, t_i) : Y \times T \rightarrow \Re^+ \tag{2}$$

Thus, loss of cross-entropy

$$loss = -\sum_i t_i \log y_i \tag{3}$$

The major component of the Deep Learning Convolution Neural Network is convolution layers, Pooling, Activation unit, Batch normalization, fully connected layers, and proposed Huddle PSO for fitness evaluation function.

4.2. Convolutional layer

The essential operation of the convolutional neural network is convolution, which let to retrieve unique information based on input. The mathematical operation involves using a sequence of filters on the set of regions in the convolution of the given input via a sliding window for obtaining a conventional feature map. The input of the feature map is stated by Eq. (4)

$$x_i^{l-1} \in \Re^{M_l \times Q_l} \tag{4}$$

and the output is given by (5)

$$x_i^{l-1} \in \Re^{H_l \times W_l} \tag{5}$$

of layer l, to achieve x_i^l all the $x_i^{l-1}$is convoluted to the equivalent kernel w_{ij}^lfurthermore, output is added to the bias $bias_j^l$. The equation for the convolutional layer is given as

$$x_j^l = f\left(\sum_{i \in M_j} x_i^{l-1} * w_{ij}^l + bias_j^l\right) \tag{6}$$

Where, i denotes the $(l-1)$layer map is linked to (j)map in the given (l)layer.

4.3. Activation function

The proposed model verifies all possible processing that familiarises the nonlinearity application. Validates its performance with a convolutional neural network and identifies its convolutions factor. The widely used ReLU function as an activation function is due to better performance in the learning process. The significant advantages are less computation cost and a high gradient convergence rate. The ReLU function is given by Eq. (7)

$$\varphi(x) = \text{maximum}(0, x) \tag{7}$$

the output value of neuron (i) of layer (k) is represented by Eq. (8)

$$x_{(i)}^{(k)} = \varphi\left(x_{(i)}^{(k-1)}, 0\right) \tag{8}$$

Pooling layer

The pooling layer minimizes the sizes of the specific cards achieved in the convolution process, thereby maintaining the required information. The pooling layer tries to reduce the number of computations and parameters to be used in the network, which in turn allows managing the overfitting. The pooling operation is performed by using a window of size $h_{pooling} \times h_{pooling}$ with movement of stride $(s_{pooling})$ on feature map. It is broadly categorized into two types,

Maximum pooling: At each level of the pooling window, it writes the maximum local value.

Average pooling: A separate pooling window local average value is calculated.

4.4. Batch normalization layer

The convergence rate is increased during the training process using Batch Normalization (BN) techniques. It holds the variance and normalizes on average output of the given convolution neural network.

Provided a mini batch $B = \{x_1, x_2, x_3 \ldots x_n\}$ of the batch size (n) and the normalized value is given by $\{\hat{x_1}, \hat{x_2}, \hat{x_3}, \ldots \hat{x_n}\}$and the equation of linear transformation, thus Batch normalization is given by (BN_γ). The transformation (β) is denoted by β: $x_1, x_2, x_3 \ldots x_n \rightarrow y_1, y_2, y_3 \ldots y_n$(9) and is calculated as

$$\mu_B = \frac{1}{n}\sum_{i=1}^{m} x_i \tag{10}$$

$$\sigma_B^2 = \frac{1}{n}\sum_{i=1}^{n} (x_i - \mu_B)^2 \tag{11}$$

$$\hat{x_i} = \frac{x_i - \mu_B}{\sqrt{\sigma_B^2 + \varepsilon}} \tag{12}$$

$$y_i = \gamma \hat{x_i} + \beta \equiv BN_{\gamma \cdot \beta}(x_i) \tag{13}$$

Where $\mu_B$the mini batch mean and $\sigma_B^2$is the variance, (β) and (γ) learnable parameters through back propagation. (ε) a positive value.

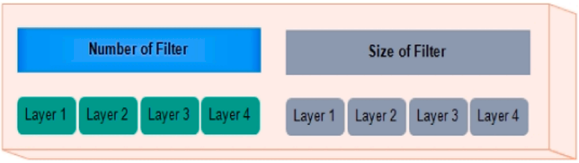

Fig. 1.2. Chromosome Definition.

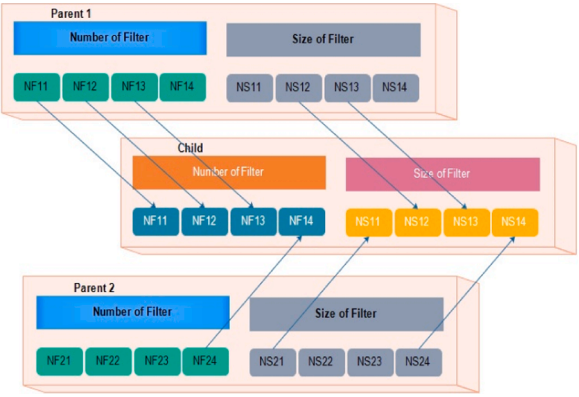

Fig. 2. Crossover operation.

4.5. Fully connected layers

Based on fully connected input neurons to the other neurons in the existing layer. It helps to identify the process and creates an output vector of K dimensions. Thus K denotes the number of classes that need to predict various pneumonia. The vector holds the classification probabilities for each category of the sample image. The prominent role of fully connected layers is identifying the link between classes and pictures. Let us consider two consecutive layers stated by Eqs. (14) and (15).

$$l^{(k-1)} \in \Re^{m^{(k-1)x1}} \tag{14}$$

$$l^{(k)} \in \Re^{m^{(k)x1}} \tag{15}$$

The corresponding weight matrix which is connected to the neurons is represented as

$$w^{(k)} \in \Re^{m^{(k-1)} \times m^{k}} \tag{16}$$

Thus the output of the fully connected layer is denoted as

$$output^{(k)} = \phi_{(k)}\left(x^{(k-1)}\right)^{T} w^{(k)} + b^{(k)} \tag{17}$$

Once evaluation gets processed, the class probabilities using input X-ray image samples and the fully connected layer are forwarded to the softmax function using the Eq. (18)

$$softmax(z)_j = \frac{e^{z_j}}{\sum_{k=1}^{k} e^{z_k}}; j = 1, \ldots, k \tag{18}$$

Where $z = [z_1, z_2, z_3, z_4 .. z_k]$ states the softmax function input vector and the output of softmax $(z)_j$ in the ranges from (0, 1, 2, 3, 4…7) depending upon the number of classes.

4.6. Genetic algorithm

A genetic algorithm (GA) is one of the heuristic search algorithms for generating offspring. It uses biological evolution similarity of fittest crossing-over techniques. Periodically fitness functions for the previous population and offspring results are evaluated regularly. Generally, a small portion of people removes the lowest fitness and initiates crossover with the highest fitness value chromosomes. Unique process identification is mainly used to achieve the best offspring and is iterative. Based on the threshold value or number of iterations stopping criteria need to be mentioned explicitly. Otherwise, GA could result in no optimization.

Encoding a problem as chromosome

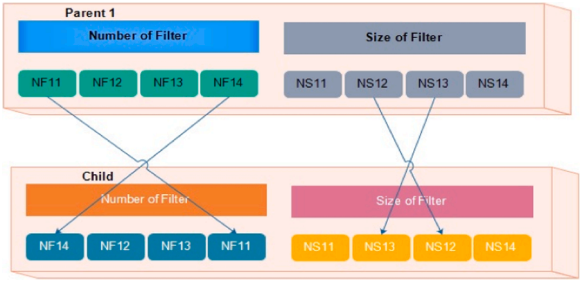

Fig. 3. Mutation Operation.

Defining the number of layers for the convolution neural network, the Genetic Algorithm fetches the optimal values for each layer for the size of the filter and the number of filters, as shown in Fig. 1.2. Thus the chromosomes are being defined in terms of vectors for size and number of filters. The cost value needs to be fetched and updated.

Fitness function

The dataset is trained and tested with a convolutional Neural Network generated based on the setting fetched from the chromosomes. After thorough testing, CNN brings the training data available in all modules.

Population Initialization

Population initialization occurs by randomly producing the chromosomes based on the upper limit of the filter size and the number of filters. A random number generator generates the initial population based on parameters.

Crossover function

Crossing over two-parent takes place to produce the offspring chromosome. The offspring produced are created using a bitmask whenever chromosomes are well-defined in terms of the bit string. In the current scenario, the cross-over function must be defined as the chromosomes being self-possessed of integers, as illustrated in Fig. 2. Parent1: vector of parent 1 consists of many filters. Let us consider NF11, NF12, and NF13, …..NF1n, similarly vector of size filter is represented as NS11, NS12, NS13…NS1n.

Likewise, for Parent2, the vector is created in terms of the number of filters and is denoted to us NF21, NF22, NF23, …..NF2m . Furthermore, the size of the filters is represented as NS21, NS22, NS23…NS2m.

The indices generated by the random index generator cross-over operation take place in terms of several filters [1,2] and the filter size [2,3]. The new child generation of chromosomes is processed based on indices and cross-over operation from parent 1 and parent 2.

Mutation operation

Parent 1 and parent 2 vectors under identified filters from NF11, NF12, NF13, NF14 and the size of filters vector as NS11, NS12, NS13…NS1n as shown in Fig. 3. Root parents are mutated to produce the new child chromosome using the random index generator. The example considers the number of filters as [1,4] and the size of filters as [2,3].

Selection process

Huddle Particle Swarm Optimization is a modified form of Particle Swarm Optimization. It is framed by dividing multiple swarms into sub-swarms. The individual swarm thereby computes the optimal solution, and it is easy solving for multi-constraints problems, which, in turn, leads to maintaining exploitation and exploration. The process involved in Huddle PSO are,

Creation of sub swarm

Based on the diversification techniques, the collision of particles takes place. Particles close to each other are rippled by force within the short-range, leading to the creation of sub swarm and, in turn, avoiding convergence.

Merging of sub swarm

An individual swarm finds the optimal solution using position best (pbest); thus, based on all the individual pbest, the global best solution is known as gbest. To achieve an optimal result, merge sub-swarm which are eligible to participate. The optimal solution derived from a sequential process is recognized to be a feasible solution. Calculating the velocity and position of the optimal particle solution is obtained. Eq. (21) states the speed and position of Huddle PSO.

$$Subswarm\left(vel_{(i+1)}\right) = Weight\left(vel_{(i)}\right) + c_1 r_1 (pbest_i - x_i) + c_2 r_2 (gbest - x_i) \tag{19}$$

$$subswarm\left(Pos\left(X_{(i+1)}\right)\right) = X_i + subswarm\left(vel_{(i+1)}\right) \tag{20}$$

$$Main\_swarm = \sum_{i,j=1}^{n} S_{1Vel_{(i,j)}Pos_{(i,j)}} + S_{2Vel_{(i,j)}Pos_{(i,j)}} + S_{3Vel_{(i,j)}Pos_{(i,j)}} \ldots S_{nVel_{(i,j)}Pos_{(i,j)}} \forall i,j \in n \tag{21}$$

$$HuddlePSO = \sum_{i,j=1}^{n} Main\_swarm_{(i,j)} + Sub\_swarm_{(i,j)} \tag{22}$$

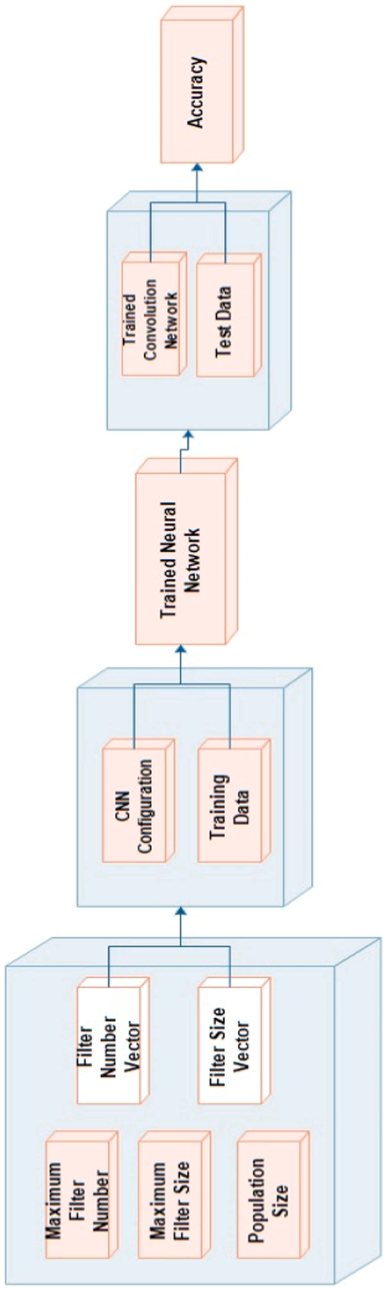

Fig. 4. System Architecture.

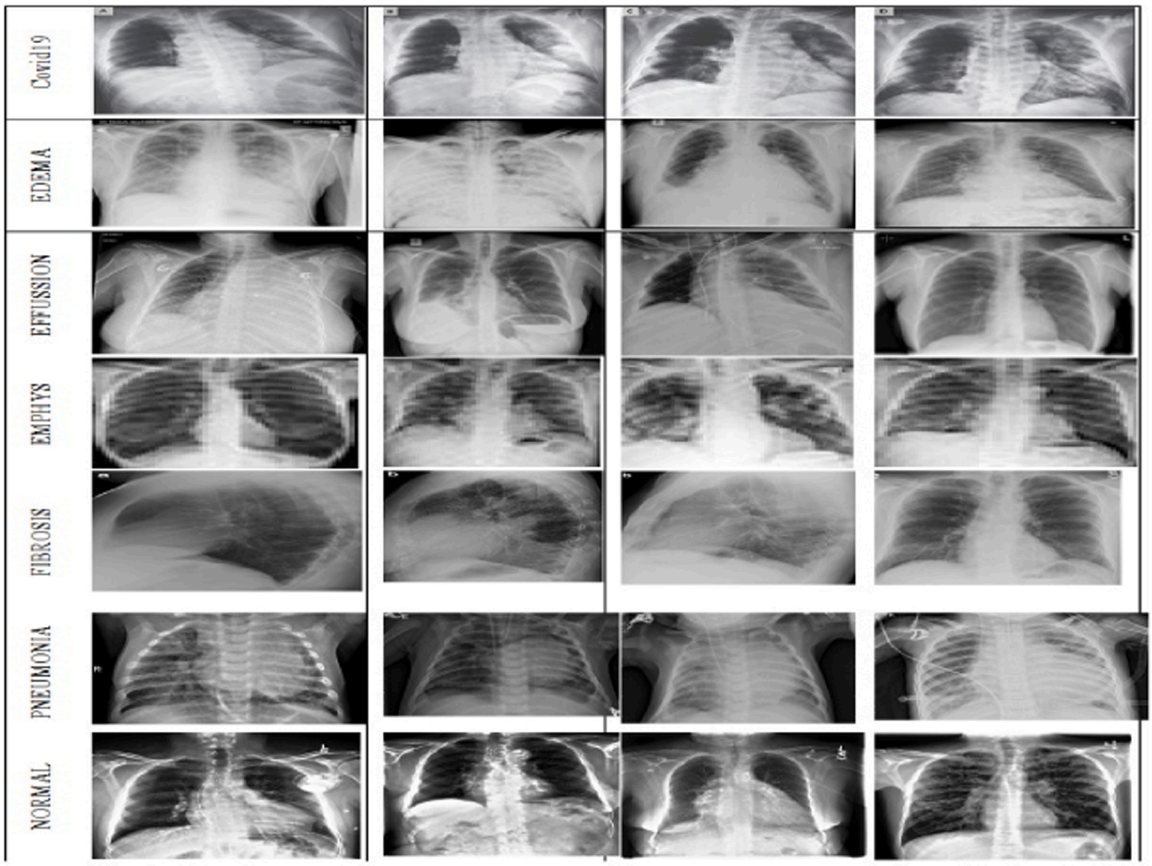

Fig. 5. Multi-level classification.

4.7. System architecture

The Fig. 4 shows the system architecture diagram of the proposed model.

1 The first block tries to create a fixed number of chromosomes based on the configuration of a convolutional neural network (CNN). Chromosomes generate the final population size with available filters in each layer. Maximum-size filters are popped out at every stage to find the top allowed filters.
2 The outcome of the new configuration design reflects based on individual convolutional neural network generation and results generated from the previous networks.

The covid19 chest X-ray image data set contains all the various types of pneumonia disease which need to be classified.

1 The training data is created based on the original data set by dividing the actual dataset into 80:20. Thus the block randomizes the selection procedure for testing and training data.
2 Train Convolutional neural network.
3 The main reason for creating CNN is based on the input and training data set. It contains fixed parameters. Some of them are the learning method (Huddle PSO), learning rate (0.001), batch size, and number of iterations (maximum epochs).
4 **Test Convolutional neural network:** It receives the complete covid19 data set and the corresponding trained network, thereby providing classification accuracy, sensitivity, specificity, f1-score, and precision as an output.

5. Experimental analysis

Prediction of Covid 19 is done using Intel i7 processor with, 512 GB of main memory, Tensor flow, 240 SSD, and 2.50 GHz with NVIDIA Tesla TitanXp GPU. The dataset consists of 5000 chest X-ray image samples such as normal chest X-ray, covid19, and other pneumonia. However, the dataset is downloaded from the Github repository. The Fig. 5 shows the multi-level classification of COVID-19, normal and other pneumonia.

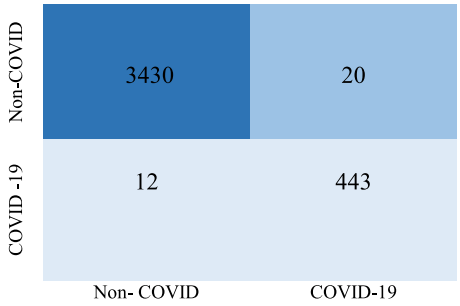

Fig. 6. Confusion Matrix.

Table 1
Confusion Matrix.

Sl.No.	Disease Name	COVID-19	Effusion	Edema	Emphys	Pneumonia	Fibrosis	Normal
1	COVID-19	443	4	1	4	3	7	1
2	Effusion	2	161	31	58	0	37	0
3	Edema	1	36	232	34	0	11	0
4	Emphys	3	54	12	156	0	40	0
5	Pneumonia	1	0	0	0	907	1	0
6	Fibrosis	3	56	17	63	0	184	0
7	Normal	2	0	0	0	0	0	1340

Dataset

Generally, the Dataset is collected worldwide and based on publications on the prediction of covid19 using chest X-ray samples. Due to available data sets, Dataset would get medical approval from government-approved practitioners for ethical clearance. Data are verified for their labeled and certified by the specialist radiologist. The models consist of anterior-posterior parts of the lungs images. The Dataset is divided into testing and training data, 3,040 chest X-ray images as the testing data set, and 2,031 as training data. The dataset is downloaded from a publicly accessible GitHub repository.https://github.com/shervinmin/DeepCovid/tree/master/data. Basically, the dataset is developed from chexpert dataset which consists of covid19 chest X-ray samples and normal chest images. A few parameters included in the dataset are sex and age. It mainly identifies which age group is getting affected more, severity level, and recovery rate. Considering age, due to less reliability above 71years, chest X-ray images sample of covid19 patients are not considered.

The sample size is increased by using data augmentation such as flipping, rotation, negligible distortion, and over-sampling, as illustrated in Fig. 5. ChexPer dataset initially consists of 2,24,316 chest X-ray images collected from 65,240 patients. The samples contain 14 categories of bacterial pneumonia, covid19, ARDS, MERS, influenza, klebsiella, fungal pneumonia, lipoid, legionella, mycoplasma, viral pneumonia, pneumocystis, pneumonia, SARS, and streptococcus.

Data Limitation

Dataset collected contains only a few samples of infected COVID-19 cases. Moreover, the patient who is affected severely also needs to be analyzed. Some patients are quarantined without adequately testing them, and patients with mild symptoms are entirely missing. There is no identification of coronavirus with whom pneumonia samples are collected. In the final process, the risk issue associated with the patient is not accessible, and the demographic characteristic is also dealt with access restrictions.

Accuracy

Accuracy is the significant metric for evaluating the proposed classification model and states whether the proposed model is suitable. It is the number of images classified correctly to the total number of chest X-ray image samples.

$$Accuracy = \frac{Number\_of\_images\_classified\_correctly}{Total\_number\_of\_images} \tag{23}$$

Specificity

Specificity generally relates to assessments correctly rejecting the healthy without any condition. The specificity test states amount of regular patients without any diseases. If and only if all medical diagnosing tests show negative.

$$\frac{True\_Positive}{True\_Positive + False\_Negative} \tag{24}$$

Sensitivity

Sensitivity states the ability to test the patient correctly and identify the disease.

$$Sensitivity = \frac{Number\_of\_True\_Positive}{Total\_number\_of\_sick\_individual\_population} \tag{25}$$

Table 2
Performance comparison.

Sl.No.	Model	COVID -19	Other	healthy	Total	accuracy	Sencitivity	Specificity	Precision	Recall	F1-score
1	MobileNet	224	700	504	1428	93.00	98.66	96.46	94.5	98.660	96.32
2	COVID-Net	53	5526	8066	13645	92.00	93.3	92.5	93.24	93.3	95.4
3	SVM	25	25	25	50	95.00	95.52	91.00	93.5	95.52	93.7
4	COVID-Net	25	-	25	50	90.00	91.0	92.1	100.0	91.0	93.5
5	ResNet50	50	-	50	100	98.00	52.5 9	99.8	98.9	52.5 9	68.6
6	InceptionResNetV2	777	-	708	1485	86.00	70.7	98.38	84	70.7	76.8
7	M-Inception	195	0.00	258	453	82.00	82.1	87.0	83.3	82.1	77.0
8	Backbone network	313	0.00	229	542	90.00	90.0	91.7	93.1	90.0	91.5
9	ResNet + Location Attention	219	224	175	618	86.00	90.0	90.3-	96.4	90.0	91.5
10	DarkCovidNet	250	500	1000	1750	92.00	94.76	95.3	98.03	94.76	96.51
11	COVNet	1296	1735	1325	4356	96.00	95.3	96.0	96.3	95.3	94.7
12	RessNet	357	1353	-	1710	86.00	90.0	91.2	93.1	90.0	93.1
13	GDCNN+HUDDLE_PSO	443	1127	3430	5000	97.23	98.62	97.0.	93.0	98.62	96.37

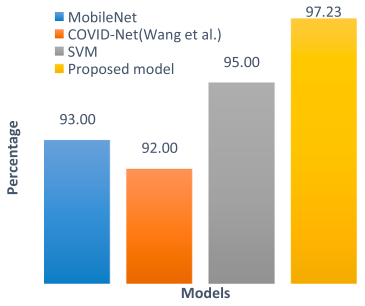

Fig. 7. Accuracy comparison.

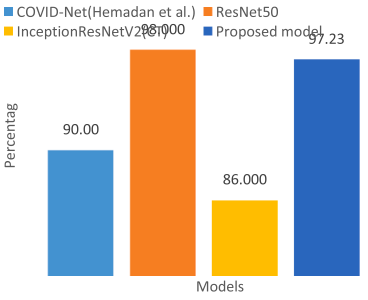

Fig. 8. Accuracy comparison.

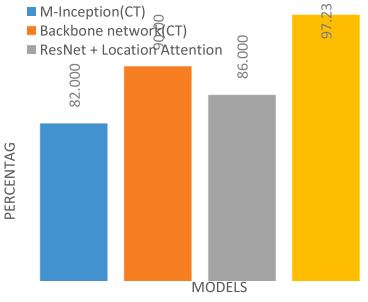

Fig. 9. Accuracy comparison.

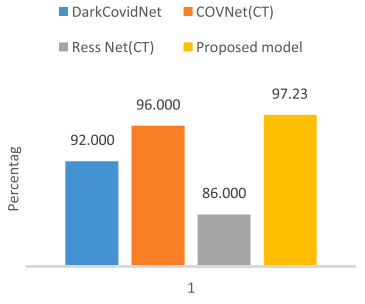

Fig. 10. Accuracy comparison.

Precision

Precision defines the sum of all the true positives (TP) to the sum of all the True Positives (TP) and all the False Positives (FP).

$$Precision = \frac{sum\_of\_all\_True\_Positive}{sum\_of\_all\_True\_Positive + All\_False\_Positives} \tag{26}$$

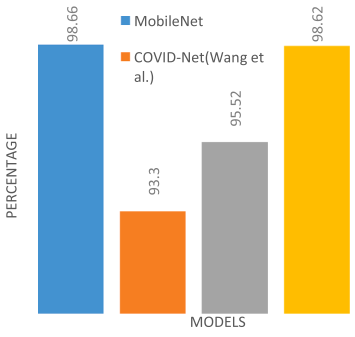

Fig. 11. Sensitivity comparison.

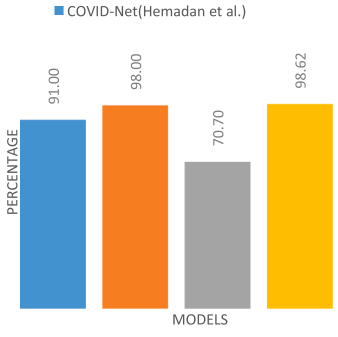

Fig. 12. Sensitivity comparison.

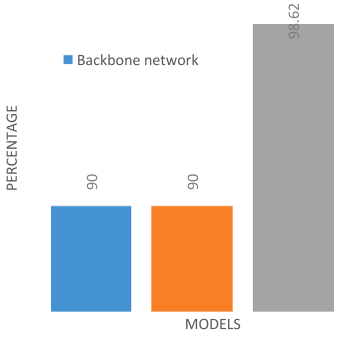

Fig. 13. Sensitivity comparison.

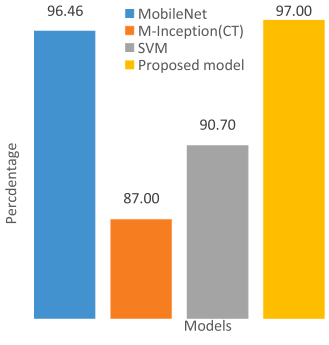

Fig. 14. Specificity comparison.

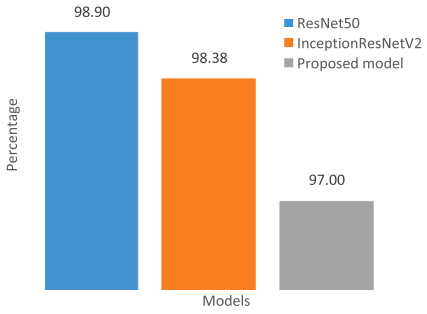

Fig. 15. Specificity comparison.

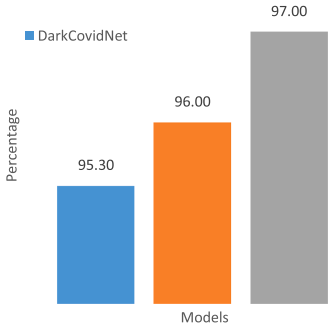

Fig. 16. Specificity comparison.

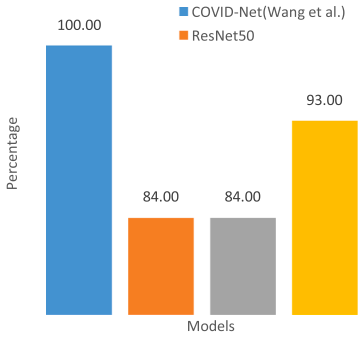

Fig. 17. Precision comparison.

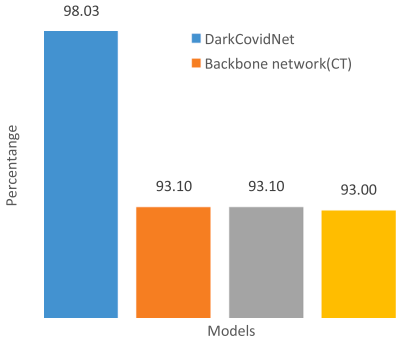

Fig. 18. Precision comparison.

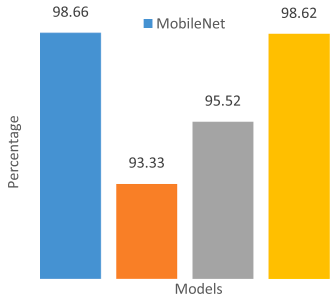

Fig. 19. Recall comparison.

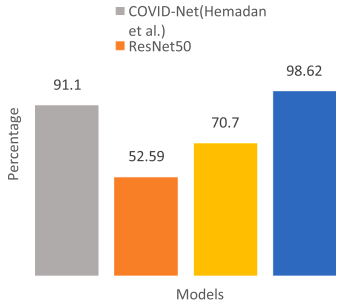

Fig. 20. Recall comparison.

Recall

The recall is defined as the sum of the true positive to the summation of True Positives and False Negative.

$$\text{Recall} = \frac{sum\_of\_all\_True\_Positives}{sum\_of\_all\_True\_Positives + All\_False\_Negatives} \tag{27}$$

F1-score

The F1-score states that twice the product of Precision and Recall to the sum of Precision and Recall.

$$F1 - score = \frac{2 \times \text{Precision} \times \text{Recall}}{\text{Precision} + \text{Recall}} \tag{28}$$

Confusion Matrix

The model's complete performance is stated in the confusion matrix, and the output illustrates as a matrix. From the Fig. (6) confusion matrix, it is clear that 20 out of 5000 image samples can have COVID-19, and 12 models indicate that people will possibly have COVID-19. In general, 3430 illustrations depict that people are not affected, that is, an average person and confirmed people affected by COVID-19 are 443. Table 1 states that the proposed method's confusion matrix table performed multi-level classification. Based on samples, multi-level classifications are performed to identify COVID-19, healthy and other pneumonia.

Table 2

Fig. 7 states the bar graph comparison of the proposed model with the other existing models. Among the various models proposed model outperformed well with an accuracy of 97.23%, whereas, MobileNet, with 93.0 accuracies, COVID-Net submitted by Wang et al. with an accuracy of 92%, is achieved. Support Vector Machine (SVM) 95% accuracy is achieved. Fig. 8 details the bar graph comparison of various models such as COVID-Net proposed by Hamadan et al., ResNet50, Inception, and ResNetV2 for CT images and proposed models. The proposed model has an accuracy of 97.23%, whereas ResNet50 has a higher accuracy of 98%, mainly due to the limited dataset used in prediction.

Fig. 9 details the accuracy compared with the various existing models in the form of a bar graph. M-Inception and Backbone network take CT images as input and perform with 82% and 90% accuracy, respectively. ResNet+Location Attention with an accuracy of 86.0%. Thus the proposed model performed better, with an accuracy of 97.23%. Fig. 10 compares the various models with the proposed model, considering CT and chest X-ray images as input. COVNET and Ress Net use CT images to predict COVID-19 with an accuracy of 96.0% and 86.0%. DarkCovidNet has an accuracy of 92.0%, whereas the proposed model has 97.23%. Fig. 11 represents the sensitivity bar graph comparison of various existing models with the proposed model. MobilNet, and the Proposed model with the same sensitivity of 98.6%, whereas COVID-Net offered by Wang et al. with a sensitivity of 93.3% and Support Vector Machine of 95.52% is achieved.

Fig. 12 depicts a bar graph comparison of the sensitivity of various models. COVID-Net was proposed by Hemadan et al. with a sensitivity of 91%, ResNet50 of 98% this is due to the limited data set used. InceptionResNetV2 model uses CT image as an input

Table 3
Accuracy comparison based on no. trails.

Sl.No	Aposto lopoulus et al. [2021]	Wang et al. [2020]	Sethy et al. [2022]	Hemadan et al. [2020]	Narin et al. [2020]	Song et al. [2022]	Wang et al. [2021]	Zheng et al. [2022]	Xu et al. [2020]	Ozturk et al. [2022]	Li et al. [2022]	Butt et al. [2022]	Proposed model
1	94.00	92.00	95.00	91.00	99.00	86.00	81.00	91.00	85.00	92.00	97.00	85.00	95.00
2	93.00	91.00	93.00	92.00	97.00	87.00	83.00	91.00	87.00	91.00	98.00	87.00	98.00
3	92.00	92.00	93.00	89.00	98.00	87.00	82.00	91.00	86.00	91.00	97.00	86.00	98.00
4	94.00	91.00	95.00	90.00	100.0	85.00	81.00	91.00	85.00	92.00	98.00	85.00	95.00
5	93.00	93.00	93.00	89.00	97.00	88.00	81.00	91.00	87.00	92.00	98.00	85.00	96.00
6	92.00	91.00	94.00	90.00	99.00	88.00	84.00	89.00	85.00	92.00	95.00	87.00	98.00
7	92.00	91.00	96.00	89.00	99.00	87.00	80.00	90.00	86.00	93.00	96.00	87.00	96.00
8	92.00	93.00	96.00	89.00	97.00	86.00	84.00	91.00	86.00	91.00	94.00	87.00	95.00
9	92.00	91.00	93.00	91.00	96.00	87.00	81.00	89.00	85.00	93.00	96.00	87.00	96.00
10	92.00	91.00	96.00	91.00	96.00	87.00	81.00	89.00	85.00	91.00	94.00	85.00	98.00
Average	92.60	91.60	94.40	90.10	97.80	86.80	81.80	90.30	85.70	91.80	96.30	86.10	96.50

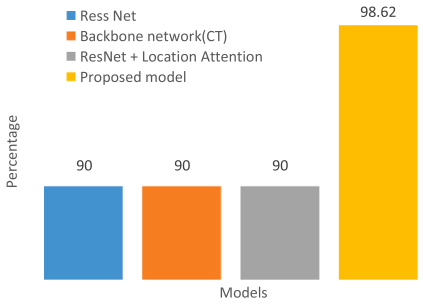

Fig. 21. Recall comparison.

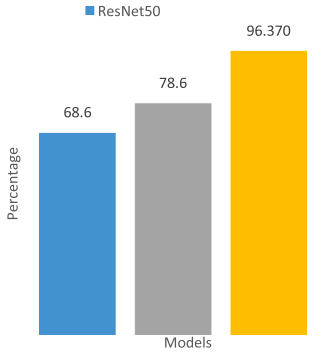

Fig. 22. F1-Score comparison.

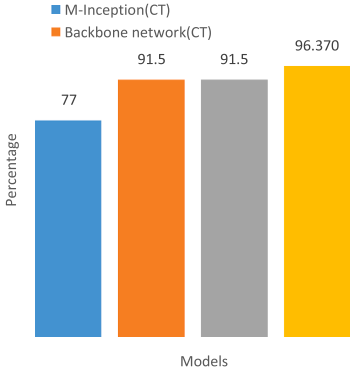

Fig. 23. F1-Score comparison

performed with a sensitivity of 70.70%. The proposed model with a better sensitivity of 98.62%.

Fig. 13 compares the sensitivity bar graph with other models, such as the Backbone network, ResNet+Location Attention, and the proposed model. The proposed model performed with better sensitivity of 98.62%, whereas both Backbone network and ResNet + Location. Attention with a sensitivity of 90% is achieved. Fig. 14 states the bar graph comparison of specificity with various existing models. The models such as MobileNet, Support Vector Machine (SVM), and the proposed model take chest X-ray images as an input, whereas, M-Inception takes CT images as an input. The proposed model outperformed well with a specificity of 97.0%. Other models with 96.46 % for MobilNet, 87% for M-Inception, and 90.70% for SVM.

Fig. 15 shows the specificity comparison in the form of a bar graph for various models like ResNet50, InceptionResNetV2, and the proposed model. Specificity for all the other model is high such as 98.90% for ResNet50, 98.83% for InceptionResNetV2. The proposed model with a specificity of 97.0%, and the main reason for low performance is the size of the dataset used in the prediction. Fig. 16 describes the bar graph comparison of specificity for models such as DarCovidNet, COVNet, and the proposed model. COVNet takes CT images as input, whereas DarkCovidNet and the proposed model take chest X-ray images. Better specificity is seen in the proposed model (97.0%) compared to the other two existing models, 95.30% for DarkCovidNet and 96.0% for COVNet.

Fig. 17 represents the bar graph comparison of precision for models such as COVID-Net proposed by Wang et al., ResNet50,

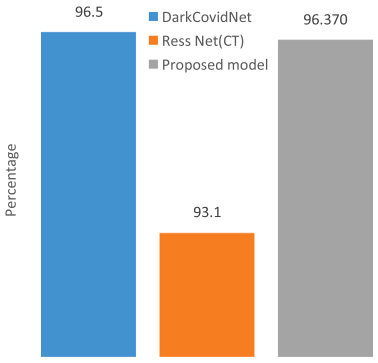

Fig. 24. F1-Score.

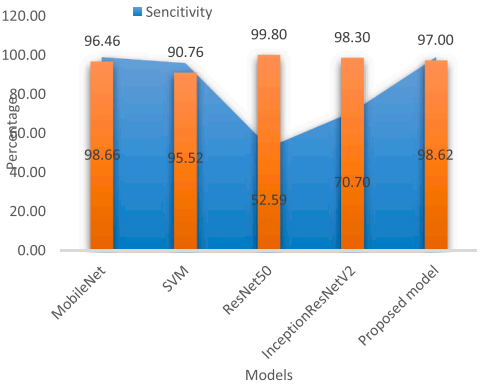

Fig. 25. Performance Comparison Sencitivity.

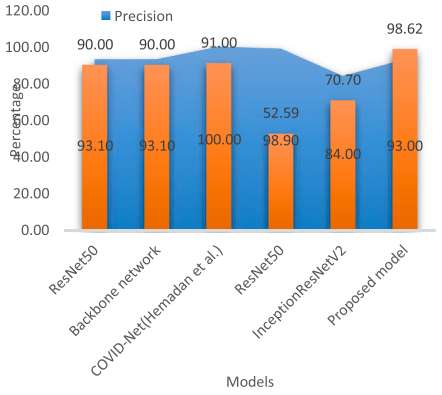

Fig. 26. Performance Comparision Precision.

InceptionResNetV2, and the proposed model. The highest accuracy is achieved for COVID-Net at 100%, whereas ResNet50 and InceptionResNetV2 with 94.0%. Moreover, the proposed model with a precision of 93% is achieved. Fig. 18 states the comparison graph of precision of various existing models, DarkCovidNet with the highest accuracy of 98.03%, whereas the proposed model, Backbone network, and ResNet with 93% precision is achieved. The primary factor with the Backbone network and ResNet is that it takes CT images and input. But in the case of other chests X-ray images are given as input. Fig. 19 details the recall bar graph comparison for MobileNet, COVID-Net, SVM, and the proposed model. MobileNet and the proposed model with a recall of 98.6% are achieved, whereas for COVID-Net proposed by Wang et al. and SVM with 93.33% and 95.62%, respectively. Fig. 20 shows the bar graph comparison of COVID-Net proposed by Hemadan et al., ResNet50, InceptionResNetV2, and the proposed model. The proposed model performed much better with a recall of 98.62% whereas, COVID-Net with 91.1%, InceptionResNetV2 of 70.7%, and ResNet50 with 52.59 % of recall. Among all ResNet50 has the minimum recall. The average performance of various researchers' techniques to predict the infected region in healthcare is illustrated in Table 3. Where the proposed multi-level classification technique improves in

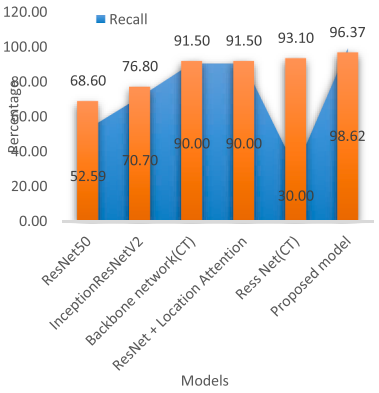

Fig. 27. Performance Comparision Recall.

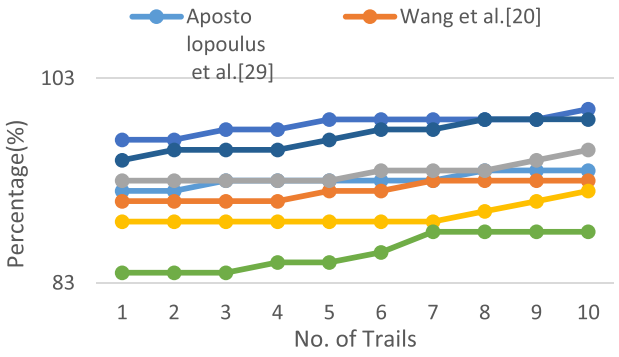

Fig. 28. Accuracy comparison based on trails.

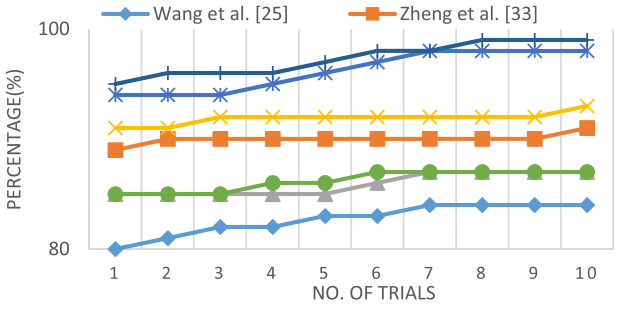

Fig. 29. Accuracy comparison based on trails.

effectiveness under all circumstances.

Fig. 21 details the comparison in the form of a bar graph for various models. The proposed model outperformed with 98.62% of recall, whereas the rest of the models, like ResNet and Backbone Network, take the input CT images, and ResNet +Location Attention with 90% recall is achieved. Fig. 22 represents the bar graph comparison of F1-score for ResNet50, InceptionResNetV2, and the proposed model. InceptionResNetV2 takes CT images as an input, whereas ResNet50 and the Proposed model take chest X-ray images as an input. High F1-score of 96.37 is achieved for proposed model, ResNet50 with 68.6% and InceptionResNetV2 of 78.6% is obtained. Fig. 23 depicts the F1-score comparison in the form of a bar graph for models like M-Inception, Backbone network, ResNet + Location Attention, and the proposed model. Among the other proposed model, 96.37% of the F1-score and the rest of the model, 77%, 91.5%, and 91.5%, are obtained. Fig. 24 shows the bar graph comparison of the F1-score for DarkCovidNet, Ress Net, and the proposed model. Ress Net uses CT images as an input, whereas, DarkCovidNet and Proposed model chest X-ray images are used as an input. Ress Net with a minimum F1-score of 93.1%, whereas, DarkCovidNet and the proposed model achieved an F1-score of 96%, respectively. Fig. 25 states the combo graph of sensitivity and specificity comparison, and it is clear from the comparison that specificity outperforms 98.62% for the proposed model than the sensitivity of 97.0%. The main reason for the increased sensitivity for the existing models is the smaller dataset used. Fig. 26 shows the combo graph comparison of Precision and recall, and the proposed model

precision performed better with 98.62 and recall of 93.0%. Among the existing model, COVID-Net presented by Hemadan et al. performed better for recall with 100% as it used CT image as an input. Fig. 27 describes the combo graph comparison of the Recall versus the F1-score. The comparison is made with all the existing models along with the proposed model. The proposed model performed well, with a recall of 98.62% and an F1-score of 96.37%. Table 3 accurately compares the number of trials with the existing methods. Figs. 28 and 29 state the accuracy comparison based on the existing method with the proposed method for 10 trials. The proposed method outperforms well compared with existing models.

The major advantage of the proposed models are

- The proposed model performs well in the early detection of COVID-19, edema, fibrosis, effusion, emphysema, pneumonia, and typical classification problems using input as chest X-ray image samples.
- The GDCNN model successfully predicts COVID-19 with an accuracy of 97.23%, sensitivity of 98.62%, specificity of 97.0%, and precision of 93.0%.
- It acts as a tool for radiologists in the earlier prediction of COVID-19.

6. Conclusion

The GDCNN model helps to improve the prediction and early diagnosis of COVID-19. The proposed model performs multi-class classification of COVID-19, edema, fibrosis, effusion, emphysema, pneumonia, and normal, which helps classify accurately between the infected patient and normal patient using the chest X-ray image samples. Training the publicly available 5000 chest X-ray dataset using GDCNN gives effective learning. With an accuracy of 97.23%, sensitivity 98.62%, specificity 97.0%, precision 93.0%, recall 98.62%, and F1-score 96.37%. The model exhibits promising and superior performance in classifying various pneumonia.

Furthermore, the GDCNN model is a tool for radiologists and clinicians for early detection of COVID-19 within a short time interval at a low cost. Future work focuses on detecting various lung diseases. It plans to train the model with more image samples, predict conditions with CT images, and compare the result with X-ray images.

Declaration of Competing Interest

We wish to draw the attention of the Editor to the following facts which may be considered as potential conflicts of interest and to significant financial contributions to this work. [OR] We wish to confirm that there are no known conflicts of interest associated with this publication and there has been no significant financial support for this work that could have influenced its outcome.

We confirm that the manuscript has been read and approved by all named authors and that there are no other persons who satisfied the criteria for authorship but are not listed. We further confirm that the order of authors listed in the manuscript has been approved by all of us.

We confirm that we have given due consideration to the protection of intellectual property associated with this work and that there are no impediments to publication, including the timing of publication, with respect to intellectual property. In so doing we confirm that we have followed the regulations of our institutions concerning intellectual property.

We understand that the Corresponding Author is the sole contact for the Editorial process (including Editorial Manager and direct communications with the office). He/she is responsible for communicating with the other authors about progress, submissions of revisions and final approval of proofs. We confirm that we have provided a current, correct email address which is accessible by the Corresponding Author and which has been configured to accept email from s.srinivasalu.1@elsevier.com/DIB@elsevier.com.

Data availability

Data will be made available on request.

References

[1] Goundar S, Deb A, Goel L, Naseem M. Using online student interactions to predict performance in a first-year computing science course. Technol, Pedagogy Educ 2022. https://doi.org/10.1080/1475939X.2021.2021977.
[2] Hasan MK, Akhtaruzzaman M, Kabir SR, Gadekallu TR, Islam S, Magalingam P, Alazab MA. Evolution of industry and blockchain era: monitoring price hike and corruption using BIoT for smart government and industry 4.0. IEEE Trans Ind Inf 2022.
[3] Asghar U, Arif M, Ejaz K, Vicoveanu D, Izdrui D, Geman O. An improved COVID-19 detection using GAN-based data augmentation and novel QuNet-based classification. Biomed Res Int 2022;2022:9. https://doi.org/10.1155/2022/8925930. Article ID 8925930pages.
[4] Hasan MK, Islam S, Memon I, Ismail AF, Abdullah S, Budati AK, Nafi NS. A novel resource oriented DMA framework for internet of medical things devices in 5G network. IEEE Trans Ind Inf 2022.
[5] Ejaz K, Arif M, Shafry Mohd Rahim M, Izdrui D, Craciun DM, Geman O. Confidence region identification and contour detection in MRI image. Comput Intell Neurosci 2022;2022:13. https://doi.org/10.1155/2022/5898479. Article ID 5898479pages.
[6] Izdrui D-R, Hagan MG, Geman O, Postolache O, Alexandre R. Chapter 11 - Smart sensing systems for in-home health status and emotional well-being monitoring during COVID-19, Editor(s): Valentina E. Balas, Oana Geman, Guojun Wang, Muhammad Arif, Octavian Postolache, Biomedical Engineering Tools for Management for Patients with COVID-19. Academic Press; 2021. p. 173–86. ISBN 9780128244739.
[7] Shankar A, Dayalan R, Chakraborty C, et al. Correction to: a modified social spider algorithm for an efficient data dissemination in VANET. Environ Dev Sustain 2022. https://doi.org/10.1007/s10668-022-02146-4.
[8] Hasan MK, Alkhalifah A, Islam S, Babiker N, Habib AKM, Aman AHM, Hossain M. Blockchain technology on smart grid, energy trading, and big data: security issues, challenges, and recommendations. Wirel Commun Mobile Comput 2022:2022.

[9] Chinnasamy S, Naveen J, Alphonse PJA, Dhasarathan C, Sambasivam G. Energy-aware multilevel clustering scheme for underwater wireless sensor networks. IEEE Access 2022;10:55868–75. https://doi.org/10.1109/ACCESS.2022.3177722.
[10] Ai T, Yang Z, Hou H, Zhan C, Chen C, Lv W, Tao Q, Sun Z, Xia L. Correlation of chest CT and RT-PCR testing in coronavirus disease 2019 (covid-19) in china: a report of 1014 cases. Radiology 2020:200642.
[11] Dhasarathan C, Shrestha H, et al. An NLP based sentimental analysis and prediction: a dynamic approach. Communication, Networks and Computing. CNC 2020. Communications in Computer and Information Science. Singapore: Springer; 2021. https://doi.org/10.1007/978-981-16-8896-6_28. vol 1502.
[12] Fang Y, Zhang H, Xie J, Lin M, Ying L, Pang P, Ji W. Sensitivity of chest ct for covid-19: comparison to rt-pcr. Radiology 2020:200432.
[13] Wang L., Lin Z.Q. and Wong A. COVID-net: a tailored deep convolutional neural network design for detection of COVID-19 cases from chest x-ray images. arXiv, Mar. 2020.
[14] Hemdan E.E., Shouman M.A., Karar M.E. Covidx-net: a framework of deep learning classifiers to diagnose covid-19 in X-ray images. arXiv preprint arXiv:2003.11055. 2020 Mar 24.
[15] Kumar P. and Kumari S. Detection of coronavirus disease (COVID-19) based on deep features. preprints.org, no. March, p. 9, Mar. 2020.
[16] J. Chen, L. Wu, J. Zhang, L. Zhang, D. Gong, Y. Zhao, S. Hu, Y. Wang, X. Hu, B. Zheng, et al., Deep learning-based model for detecting 2019 novel coronavirus pneumonia on high-resolution computed tomography: a prospectivestudy, medRxiv (2020).
[17] X. Xu, X. Jiang, C. Ma, P. Du, X. Li, S. Lv, L. Yu, Y. Chen, J. Su, G. Lang, et al., Deep learning system to screen coronavirus disease 2019 pneumonia, arXiv preprint arXiv:2002.09334 (2020).
[18] H. Zhang, K.M. Saravanan, Y. Yang, M.T. Hossain, J. Li, X. Ren, Y. Wei, Deep learning based drug screening for novel coronavirus 2019-ncov (2020).
[19] B.R. Beck, B. Shin, Y. Choi, S. Park, K. Kang, Predicting commercially available antiviral drugs that may act on the novel coronavirus (2019-ncov), wuhan, china through a drug-target interaction deep learning model, bioRxiv (2020).
[20] E.E.-D. Hemdan, M.A. Shouman, M.E. Karar, Covidx-net: a framework of deep learning classifiers to diagnose covid-19 in x-ray images, arXiv preprint arXiv: 2003.11055 (2020).
[21] Butt C, Gill J, Chun D, Babu BA. Deep learning system to screen coronavirus disease 2019 pneumonia. Appl Intell 2020.
[22] Babukarthik RG, Ananth Krishna Adiga V, Sambasivam G, Chandramohan D, Amudhavel J. "Prediction of COVID-19 using genetic deep learning convolutional neural network (GDCNN). IEEE Access 2020;8:177647–66.
[23] Rostami M, Oussalah M. A novel explainable COVID-19 diagnosis method by integration of feature selection with random forest. Inf Med Unlocked 2022;30: 100941. ISSN 2352-9148.
[24] Clough A, Sanders J, Banfill K, Faivre-Finn C, Price G, Eccles CL, Aznar MC, Van Herk M. A novel use for routine CBCT imaging during radiotherapy to detect COVID-19. Radiography 2022;28(1):17–23. ISSN 1078-8174.
[25] Tripathi D, Shukla AK, Reddy BR, et al. Credit scoring models using ensemble learning and classification approaches: a comprehensive survey. Wirel Pers Commun 2022;123:785–812. https://doi.org/10.1007/s11277-021-09158-9.

R.G. Babukarthik is working as an Assistant Professor in the Department of Computer Science and Engineering at Dayananda Sagar University. Focusing research on Optimization problems used for solving web service selection in cloud computing. With an experience of more than 13 years, his research area includes cloud computing, web Service, Optimization Algorithms, Deep Learning and Data science.

Chandramohan Dhasarathan received the Ph.D. degree in computer science & engineering from Pondicherry Central University, Puducherry, India, and He is currently an Assistant Professor, ECED, Computer Science and Engineering Department, Thapar Institute of Engineering & Technology, Patiala, Punjab. His area of interest includes Pervasive & Ubiquitous Computing, Privacy and Security, Blockchain Technology, Opportunistic Computing, Fog & Edge Computing, Underwater Communication.

Diwakar Prasad Tripathi, received his Ph.D from National Institute of Technology Goa, India. Currently he is working as an Assistant Professor, at Department of Electrical and Instrumentation Engineering, Thapar Institute of Engineering and Technology, Patiala, Punjab, India. His area of research includes machine learning, artificial intelligent, data mining, big data, data analytics, data science. He is having 15+ years of teaching and research experience.

Manish Kumar received his B.E degree in Information Technology from Rajiv Gandhi Technical University, Bhopal, India in 2011 and Ph.D. degree from Indian Institute of Technology (Indian School of Mines), Dhanbad in the year 2018. He is currently working as an Assistant Professor in the Computer Science and Engineering Department, Thapar Institute of Engineering & Technology, Patiala, Punjab, India. His research interest includes Soft Computing applications for Bioinformatics problems, and Computational Intelligence.

G. Sambasivam received the Ph.D. degree in computer science and engineering from Pondicherry University, Puducherry, India. He is currently working as a Senior Assistant professor in VIT-Bopal, India. He is an international academic expert and served as an Associate Dean of Research with the Faculty of Information and Communication Technology, ISBAT University Kampala, Uganda. His research interests include artificial intelligence, machine learning, and Web service computing.